IEEE Access
Multidisciplinary ⋮ Rapid Review ⋮ Open Access Journal

Received November 28, 2020, accepted December 10, 2020, date of publication December 15, 2020,
date of current version December 30, 2020.

Digital Object Identifier 10.1109/ACCESS.2020.3045055

Photonic-Radar Based Multiple-Target Tracking Under Complex Traffic-Environments

VISHAL SHARMA[1], (Senior Member, IEEE), AND LOVE KUMAR[2]
[1]Aston Institute of Photonic Technology (AiPT), Aston University, Birmingham B4 7ET, U.K.
[2]Department of Electronics and Communication, DAV Institute of Engineering and Technology, Jalandhar 144008, India

Corresponding author: Vishal Sharma (v.vishal@aston.ac.uk)

This work was supported in part by the Aston Institute of Photonic Technologies (AiPT), Aston University, Birmingham, U.K., and in part by the European Union-Sponsored H2020-MSCA-IF-EF-ST under Project 840267.

ABSTRACT Recent developments in the state-of-the-art Intelligent Transportation Systems enable autonomous vehicles to offer significant safety services to take appropriate and prompt actions to avoid any probable unfortunate road-hazard. As the utmost functions of the advanced driving assistance system-equipped autonomous vehicles governed by the equipped radar, therefore, the radar system should have the ability to track multiple-targets accurately with high radar-resolutions. Unlike the microwave-radar, the photonic-radar comes out as an attractive candidate owing to provide wide-spectra to attain improved and precise radar-resolutions at low-power requirements along with extended target-range even under severe atmospheric fluctuations. Therefore, a linear frequency-modulated continuous-wave photonic-radar is developed in this work to carry out a radar cross-section-based tracking of multiple mobile-targets in the presence of fog, cloud, and rain. Besides it, some complex real-time traffic-scenarios consisting of multiple mobile-targets make the target-detection, data-association, and classification processes more complicated. Therefore, this work is tested for different multiple-mobile targets in different complicated traffic-scenarios modeled by using MATLAB^{TM} software. The performance of the demonstrated photonic-radar is assessed through the power spectral density and range-Doppler mapping measurements. Furthermore, a comparison of the developed photonic-radar is also established with conventional microwave-radar to present a comparative analysis.

INDEX TERMS Atmospheric fluctuations, microwave-radar, photonic-radar, radar cross-section.

I. INTRODUCTION

Recently, the demands of the photonic-radar (PHRAD) technology augments significantly in the arena of smart autonomous transportation, surveillance, and navigation-related applications owing to provide wide-spectra to attain improved and precise radar-resolutions. Especially in Autonomous Vehicle (AV) industry, the laser-driven radar is being implemented to offer numerous substantial services including lane-detection, collision-evading, multiple target-detection, blind-spot monitoring, and park assistance [1], [2] to enable the self-driving vehicles to respond promptly to avoid any unfortunate road-hazard [2]–[5]. As a part of these objectives, the simultaneous and precise measurements of detection-range and velocity with target-characterization becomes essential in today's AV industry. Therefore, the AV-related industries are looking for alternative approaches to enhance the accuracy of self-driving vehicles with prolonged detection-range at low-power requirements [6], [7]. For the last few years, the photonic-radar technology proves to be an attractive candidate for intelligent transportation systems (ITS), remote-sensing, and other related surveillance industries [8]–[11]. On the other hand, the existing advanced microwave-based surveillance and navigation systems are limited to a marginal accuracy-range, especially in the populated areas at high frequencies [12], [13]. Keeping in mind the current requirements of the advanced AVs, the importance of the frequency-modulated continuous-wave photonic-radar upturns significantly and is rapidly growing at its initial phases by providing high range-speed resolution with precision along with an extended tracking range [14]–[16].

Moreover, the photonic-radar related industries start preferring to operate in the 74–77 GHz frequency band to attain high radar resolutions. However, the propagation

The associate editor coordinating the review of this manuscript and approving it for publication was Sukhdev Roy.

characteristics of the radar signals, especially in the 77 GHz frequency band, experience a significant attenuation [17] when exposed to severe atmospheric fluctuations. Absorption due to atmospheric gasses and other atmospheric elements attenuate the radar signals [18], [19] that diminish the range-visibility of the detected-objects. This leads to offer marginal information about the target's identification and location. Moreover, there are some other environmental factors, for instance, fog, cloud, rain, haze, and snow, which affect the transmission of the radar signals significantly in the mmW band.

Recent work measures the impact of dust, smoke, and other random environment variations on the performance of self-driving vehicles through simulation investigations [20], [21]. To measure the attenuation due to atmosphere- and the target-reflectivity variations, a comparative study of a laser radar is reported at different operating wavelengths [22]. It is shown that both factors have unique spectral features. Moreover, the rangefinders operating at different wavelengths are affected by specific environmental changes in different ways. As the light at 1550 nm is safe for the human eye, it is preferred to use this wavelength in the AV industries. However, due to water absorption at 1550 nm, high susceptibility to the elevated humidity, rain, fog, and wet-target is expected. Further, a demonstration of an automotive laser-driven radar is reported in the presence of exhaust gasses, ambient temperature, rain, and fog [24]–[27] that confirms the atmospheric influence over the performance of the radar. However, these works are limited to the detection of a single static target in a simple traffic environment considering weather factors separately. The earlier work of authors [28] modeled a frequency-modulated continuous-wave photonic radar established by transmitting the radar signals over the free space channel in the optical domain. This is a simple model consisting of an immobile target-object and a static radar system to measure the intensity of reflected echoes in the presence of atmospheric fluctuations in the optical domain.

Moreover, to characterize the target-objects, which is one of the essential requirements of the Autonomous Vehicle (AV) industry, it becomes mandatory to measure the target's properties and its dimensions. In this context, the authors defined a five parameters-based BRDF function by measuring the reflectance characteristics of the target-materials [29]. The demonstrated PHRAD system used the Torrance–Sparrow model to determine the BRDF function of silver-coated tinfoil material tested at different operating wavelengths and different incident angles in the optical domain. Moreover, the work is investigated to improve the storage-ability of the LiDAR cloud-point data to achieve a fast estimation of the BRDF function to measure reflection properties based on wavelength and target material. This work is also limited to a simple traffic-scenario without considering the atmospheric fluctuations. So, a detailed investigation is required to assess the influence of harsh weather situations in some complicated real-time traffic environments, including multiple targets to perform simultaneous measurements of unambiguous range and velocity.

Additionally, some authors demonstrated traffic-surveillance-related applications by considering different road traffic situations [30]–[32]. A recent demonstration [30], using an mmW radar in the 24 GHz band, is carried out to differentiate the road-structures and mobile vehicles using an M-estimator sample and Consensus (MSAC) advanced version of random sample consensus-based estimation (*RANSAC*) algorithm. Also, a radar interferometry technique [31] demonstrates a dense traffic-scenario by computing target-speeds of multiple targets by optimizing the position of the installed radar in Ka-band (35-GHz) through simulations and field-trails. However, this system can only discriminate the targets at different speeds. If two vehicles are in separate road lanes or at different distances but travel with the same velocity, this system fails. Further, the multiple target detection is performed in a random traffic-scenario using a conventional radar without explaining the detailed information of the used radar [32]. Moreover, all these demonstrated works are under clear-weather situations in [30]–[32].

Besides it, the localization of multiple targets, including low-observed targets, is also highly desirable in state-of-the-art AVs even under severe weather conditions to assess the traffic situations extensively. Therefore, considering the current needs of the AVs, the author's previous work [28], [29] is extended here to perform the simultaneous range-speed measurements using an LFMCW-PHRAD radar, developed in the 77 GHz band. Several non-complex and complex traffic-scenarios, including five automotive targets like Car, Truck, Motorbike, Bicycle, and Pedestrian, are developed and investigated under an individual and combined influence of atmospheric fluctuations. The modeled multiple targets are differentiated by their associated RCS, traveling at different speeds and different distances from the radar-equipped vehicle. All the modeled target-objects and radar-equipped vehicles are mobile in nature in this work. Furthermore, a comparison of the demonstrated photonic-radar is also presented with the conventional microwave radar to validate the robustness of the PHRAD. All the measurements are in terms of the power spectral density (PSD), beat frequency, and rang-Doppler mapping.

The demonstrated work is structured as Section I illustrates the requirements, challenging issues, and recent developments. Section II points to the main highlights of the demonstrated photonic-radar. Section III describes the modeling of LFMCW-PHRAD with the detailed system parameters. Section IV describes the modeling of target- and atmospheric-scenarios consisting of different automotive-targets distinguished in terms of their associated RCS values along with propagation channel modeling, including atmospheric variations. Section V discusses the outcomes of both the demonstrated radar systems for non-complex traffic scenarios of identical targets. Section VI-VII describes

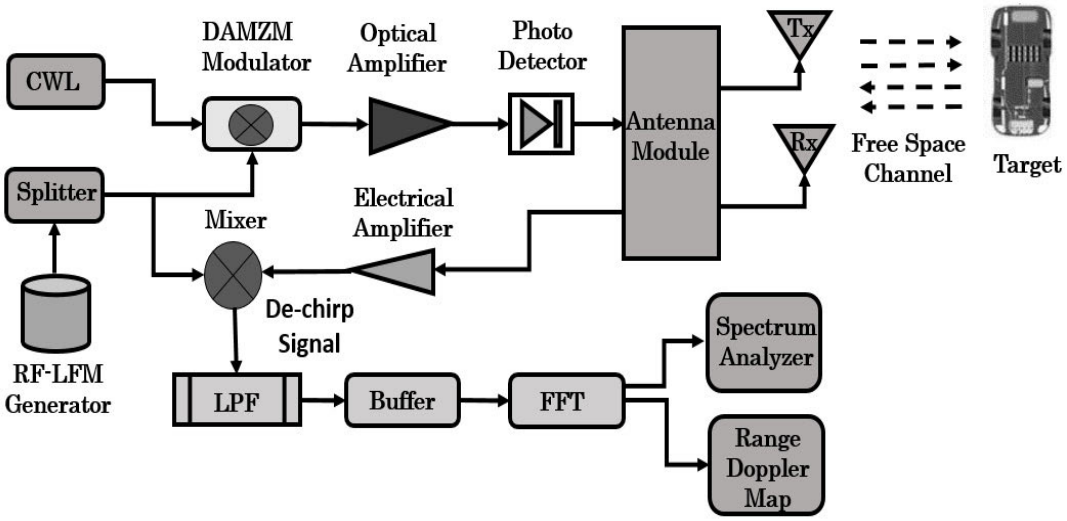

FIGURE 1. Demonstrated linear frequency-modulated continuous-wave photonic-radar (LFMCW-PHRAD).

the RCS-based measurements for non-complex and complex traffic scenarios. Section VIII concludes the presented work and presents its future extensions.

II. MAJOR CONTRIBUTION

As the radar resolution is a function of the bandwidth of the transmitted pulses, therefore, the higher is the bandwidth of the transmitted pulses, the more is the ability of the radar to differentiate the closely spaced target-objects. That is why radar manufacturers prefer the 77-GHz frequency band to the 24-GHz band. At 77-GHz, high bandwidth of ≈ 4 GHz is attainable, and at 24-GHz, it is ≈ 200 MHz. This wide-bandwidth in the 77–81 GHz frequency-band offers twenty-times better range-resolution and three-time better velocity-resolution with improved accuracy than that of the 24-GHz band [29]. Moreover, to attain high bandwidth in mmW radar systems to improve the range-and imagery-resolution, one must work at higher frequencies of mmW band where the atmospheric fluctuations dominate the radar performance significantly.

Here, the laser-driven/photonic-radar systems play a vital role. The demonstrated LFMCW-PHRAD computes the target-range and velocity measurements simultaneously of radar cross-section-based defined multiple automotive targets moving at different speeds and distances from the radar-equipped vehicle. The LFMC signals are spectrally broadened by optical modulating over the laser pulses to attain high range-and imagery resolution and then down-converted into the RF-domain to transmit over the free-space channel towards the illuminating targets. Moreover, it reduces the undesired higher-order harmonics by controlling the biasing of the optical modulator that occurs in the direct transmission of the mmW signals and deteriorates the radar performance significantly. Further, the modeled photonic-radar is investigated under some non-complex and complex road-traffic scenarios, discussed in detail in section VI–VII.

Also, to determine the performance of the demonstrated LFMCW-PHRAD for multiple target-detection in complex traffic-scenarios under atmospheric fluctuations, several scenarios, including environmental factors like Rain, Fog, and Clouds, are developed. For modeling of the LOS channel, including environmental factors, the authors refer to the ITU-R P.838–3, ITU-R P.840–6, and ITU-R P.676–11 channel model recommendations. Moreover, a comparison of the demonstrated LFMCW-PHRAD is also established with the convention radar (mmW band).

III. SYSTEM DESCRIPTION

The demonstrated PHRAD is developed, as shown in Figure 1, to perform simultaneous and unambiguous measurements of range and velocity for multiple mobile-targets in complex traffic scenarios under the impact of the various environment variations. The demonstrated LMCW-PHRAD works on the principle of the Doppler Effect, where the reflected signal is a time-delayed replica of the transmitted signal. As the transmitted frequency-modulated signal exhibits a linear sweep through a frequency-band, a constant beat frequency is attainable that further provides the time-delay and frequency-shift related information. This data-information can be translated into the detection-range and velocity measurements. In this work, an up-and-down-sweep linear frequency-modulated (LFM) waveform is considered to alleviate the range-speed decoupling effect [27], which is generated using a local waveform generator at 77 GHz [29]. These LFM signals are optically modulated over the light-pulses of a continuous-wave (CW) light-source at 1550 nm before their transmission through the free space channel. The optical modulation of RF-LFM signals over light generates

the widened optical pulses with a linear shift that can be easily monitored for upper and lower frequency [30], [31] and provides a high range-resolution. The optical modulation is achieved by employing a dual-arm Mach Zehnder (DAMZM) external optical modulator with proper biasing of both arms to generate second-order modulation sidebands by suppressing the higher-order undesired sidebands. The DAMZM modulator has two sub-arms that are embedded in one parent arm. The RF-LFM signal is applied to one arm directly and to another arm with a phase-shift of 90°. The modulated signal at the output of the DAMZM modulator is computed as [27]

$$A_0 = \frac{A_{in}}{10^{\frac{IL}{20}}}\left[\gamma \cdot e^{\left(-i\pi t \frac{v2(t)}{V_{\pi RF}} + i\pi t \frac{vbias2(t)}{V_{\pi DC}}\right)} + (1-\gamma)\cdot e^{\left(-i\pi t \frac{v1(t)}{V_{\pi RF}} + i\pi t \frac{vbias1(t)}{V_{\pi DC}}\right)}\right] \quad (1)$$

where A_{in} is the amplitude of the light signal, $v_1(t)$ and $v_2(t)$ are the electrical-voltages applied on both arms of the modulator, $v_{bias1}(t)$ and $v_{bias2}(t)$ are bias-voltages and taken as $-2V$ and $2\ V$ respectively, IL is insertion-loss, $V_{\pi RF}$ and $V_{\pi DC}$ are the switching modulation-voltage and bias-voltage respectively, and γ is power splitting-ratio calculated as $\gamma = \frac{1}{2}\left(1 - \frac{1}{\sqrt{er}}\right)$; $er = 10^{\frac{ER}{10}}$; ER is the extinction ratio.

These optically modulated wideband signals are re-converted into electric signals by attaining an optical-to-electrical conversion using a PIN photo-detector with Responsivity of 80% after the optical amplification. The optical-to-electrical converted signals are then propagated through a narrowband line-of-sight (LOS) channel towards the illuminated-targets via an antenna module. The LOS channel model, including fog-, cloud-, and rain-weather factors, is designed to investigate the developed LFMCW-PHRAD under atmospheric fluctuations. The reflected-echoes from the illuminated-targets, differentiated by their associated radar cross-section (RCS), are received with a propagation time-delay of $(2 \times R)/c$. If the transmitted electrical signal is reflected by N illuminated-targets, and the chirp is articulated as a frequency modulated signal, the received reflected-echoes can be expressed [36] as

$$r(t) = \sum_{n=1}^{N} A_n \sum_{m}^{M-1} cos\emptyset_i\,(t - mT - \tau_n)\cdot e^{-i2\pi v_n t} \quad (2)$$

where A = amplitude of the reflected echoes, M is the number of chirps with instantaneous phase $\emptyset_i.\tau_n$ and v_n are the delays corresponding to the range and Doppler-shift. The beat frequency for N illuminated-targets after the frequency down-conversion is expressed as

$$f_b(N) = \sum_{m=0}^{M-1} A_m \sum_{n=1}^{N} A_n \cdot e^{i\emptyset_{bmn}} \quad (3\text{-a})$$

$$\text{And, } \emptyset_{bmn} = \emptyset_{0mn} + 2\pi m_0 A_0 \tau_n t + 2\pi v_n t \quad (3\text{-b})$$

where A_0 is the amplitude of the modulated-signal from equation (1), $\emptyset_{0mn}$ is a constant term, and m_0 is the modulation-index.

After the proper amplification using an electrical amplifier and mixing with the RF-LFM signals via an electric mixer to attain the frequency down-conversion, the de-chirped signals are passed through a low pass filter (LPF) to retrieve the beat signal. In this work, the authors stored 128 sweeps in a buffer to extract the Doppler information as it is not feasible to it in a single sweep. Once the buffer is filled with 128 sweeps, the two-dimensional Fast Fourier transformation (2DFFT) is executed to measure the target-range and relative velocity [29], [36], [37]. The Hanning window is employed as it offers a perfect periodic extension to a windowed signal contained in the discrete Fourier transform and reduces the level of false alarm rate (FAR). The demonstrated LFMCW-PHRAD is modeled by using MATLAB^{TM}. The detailed parameters of the demonstrated laser-driven radar are illustrated in Table 1.

IV. MODELING OF TARGET AND ATMOSPHERIC SCENARIOS

Several multiple mobile-targets, like Car, Truck, Motorbike, Bicycle, and pedestrian are developed which are traveling with different velocities at different distances before the PHRAD-equipped vehicle to measure the effectiveness of the demonstrated work. The PHRAD-equipped vehicle is modeled at a speed of 100 km/hr with an assumption that all the modeled targets are approaching it in all the developed traffic-scenarios. As the RCS depends on the frequency, azimuth angle, and distance [38]–[42], a set of RCS values is required to be measured for defining different targets. Subsequently, the considered automotive targets are differentiated by their associated RCS values to develop different complex real-time road scenarios in this work.

Moreover, the RCS behavior becomes worst for small targets like pedestrians and varies at a rapid rate, particularly in near-field and as per the properties of the target material. Therefore, to reduce the complexity, an average fixed RCS value of -10 dBsm, 4 dBsm, and 7 dBsm is used for defining the pedestrian, bicycle, and motorbike, respectively, as these targets are considered as small targets. The car and truck, considered as large-sized targets, the distance dependence of RCS is taken into account to develop an empirical relation at the carrier frequency of 77 GHz, azimuth-angel of 0°, and lobe-angle of 5°, which is expressed as [43]

$$RCS_{car}\,(dBsm) = min\begin{cases} 10\log_{10}(R) + 5 \\ 20 \end{cases} \quad (4)$$

$$RCS_{truck}\,(dBsm) = min\begin{cases} 20\log_{10}(R) + 5 \\ 45 \end{cases} \quad (5)$$

Furthermore, to determine the detection-range and relative-speed at resolution of 25 cm of multiple targets under the complex traffic- and atmospheric-scenarios including fog-, cloud-, and rain- factors, a narrowband line-of-sight (LOS) channel is modeled by using the phased-array tool of MATLAB^{TM} software to attain two-way propagation of radar signals between the transmitter and illuminated targets. The LOS channel is modeled for fog + cloud (as both have

TABLE 1. Key Parameters.

Quantity	Values
CW laser	1550 nm
FM carrier frequency	77 GHz
Maximum Target Range, R	500 m
Maximum Target Velocity	250 Km/hr
Sweep-bandwidth	600 MHz
Sampling rate	600 MHz
Sweep-time	7.33 μsec
Range-Resolution	0.25 m
Optical Detector	PIN Type
Responsivity	0.8 AW^{-1}
Antenna Type	Isotropic
Dual-arm MZM (DAMZM) Optical Modulator	1. Switching RF voltage = 4 2. Switching bias voltage = -4 3. Bias voltage 1 = -2 4. Bias voltage 2 = 2 5. Extinction Ratio = 30 dB
Target Type	Automotive (Mobile)
Radar cross-section (RCS) of Targets	1. Car = 20 dBsm 2. Truck = 45 dBsm 3. Motorbike = 7 dBsm 4. Bicycle = 4 dBsm 5. Pedestrian = -10 dBsm
PHRAD-equipped Vehicle Type	1. Automotive Car (Mobile) 2. Speed = 100 Km/hr
Fast Fourier Transformation (FFT)	1. Two-dimensional 2. Range FFT-Length = 2048 3. Doppler FFT-Length = 256
Antenna Type	Isotropic
Low Pass Filter (LPF)	2 GHz
Optical Amplifier	25 dB; Noise Figure = 5 dB
Electrical Amplifier	25 dB; Noise Figure = 4.5 dB
Free Space Channel Type	Narrowband LOS

the same atmospheric phenomenon) and rainy environments following the *ITU* model recommendation of *ITU-R P.838–3* [17] and *ITU-R P.840–6* [18]. The rain attenuation model computes the specific attenuation, A_{rain} of the transmitted signals as a function of rainfall rate, signal frequency, polarization, and path elevation angle as [17]

$$A_{rain} = k \cdot R_o^{\beta}(dB/Km) \tag{6}$$

where R_o is the rainfall-rate in *mm/hr*. k, and α are the power-law coefficients that depend upon several parameters like signal-frequency, rain-drop size, and rain-temperature and can be measured as per the Marshall-palmer distribution [40]. The cloud and fog attenuation model measure the specific-attenuation, $A_{fog,cloud}$ of the transmitted signal as a function of liquid water-density, signal frequency, temperature as [18]

$$A_{fog,cloud} = \alpha\,(f) \cdot K_{wl}(dB/Km) \tag{7}$$

where K_{wl} is liquid water-density in gm/m^3, and $\alpha(f)$ is the specific attenuation-coefficient that depends on signal-frequency in $(dB/km).(gm/m^3)^{-1}$. Moreover, the results are measured at ambient temperature of 0° C without considering the impact of atmospheric gasses through-out the demonstrated work.

V. IDENTICAL TARGET-BASED MEASUREMENTS FOR NORMAL TRAFFIC SCENARIOS

This section investigates two normal traffic-scenarios, i.e. Scenario 1 and 2 employed with five identical target-vehicles, i.e. Car with RCS of 20 dBsm, under the individual and combined influence of fog, cloud, and rain at different weak-to-severe levels. In Scenario 1, a conventional FMCW-RADAR is modeled to measure the target-range and velocity simultaneously. An up-and-down-sweep linear frequency-modulated (LFM) waveform is directly propagated towards the illuminated-targets without the optical treatment as implemented in the demonstrated PHRAD. However, the same parameters are considered for modeling of the propagation channel- and target-model to establish an impartial comparison with the demonstrated radar. In Scenario 1, a normal traffic-scenario consisted of five identical target vehicles is developed in which all target-vehicles are traveling with different velocities at different distances from the radar-equipped vehicle, as shown in Table 2. Fig. 2 (a–c) shows the measured beat signals from the returning echoes of the considered targets. The impact of the individual influence of mild-rain with a rain-fall rate of 5 mm/hr (Fig. 2(a)), mild fog + cloud with liquid water-density of 1 (Fig. 2(b)), and under the combined impact of rain, fog, and cloud (Fig. 2(c)) over the intensity of the returned pulses is measured. The specific attenuation of the modeled LOS channel is calculated as a function of the considered severity level of the rain and fog [17], [18], [44].

It is observed that the considered environmental factors affect the radar detection-range significantly and become a challenging task to measure the target-range and velocity accurately over a prolonged distance. Moreover, the range-Doppler mapping shows that under the combined impact of rain, fog, and cloud, it becomes difficult to locate the accurate position of the targets as shown in Fig. 3. Moreover, Targets 1–3 almost disappear from the area-of-interest under the combined effect of the considered weather fluctuations as the target-range is reduced to 100 m only. This implies that the attainable target-range and their localization are limited to few meters only, even when large-sized automotive objects, i.e. Car, and Truck are tested under mild weather conditions. The situation will become more critical for the tracking of small illuminated-targets, i.e. pedestrians, bicycles, motorbike, traffic-lights, animals, etc which have low radar cross-section and generates marginal weak returning pulses. So, it is difficult to track them accurately from a safe observatory-distance required in the AV industry, i.e. (> 200 m).

Further, the same scenario is tested for the demonstrated PHRAD (Scenario 2) under the individual influence of rain only with the weak-to-strong regime at a rainfall rate of 10 mm/hr, 50 mm/hr, and 100 mm/hr as shown in (Figure 4–5). All the targets are moving with the same velocity at the same distances from the photonic-radar-mounted vehicle, as shown in Table 2. Moreover, the radar cross-section is also considered as 20 dBm (for a car). It is observed that a significant improvement in the intensity of the beat

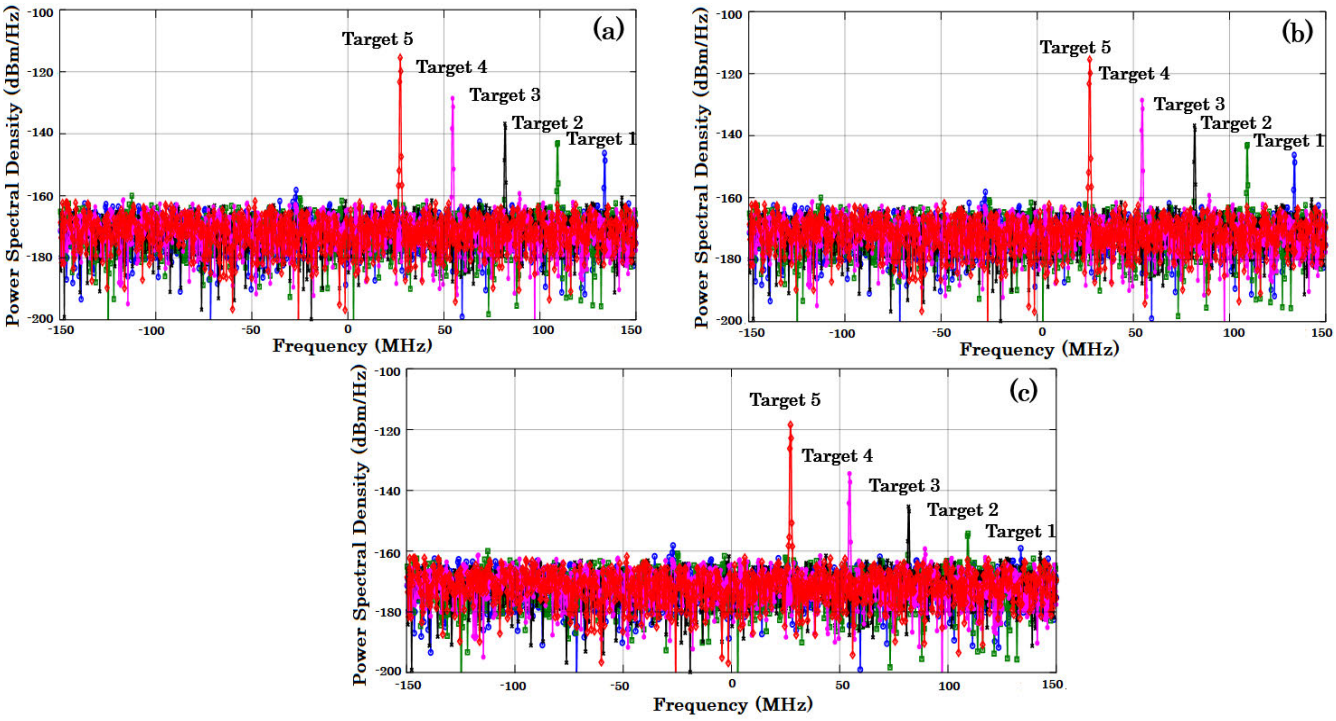

FIGURE 2. Power Spectral Density measurements of LFMCW-RADAR under the influence of (a) mild rain only, (b) mild fog + cloud, and (c) mild rain, fog, cloud for Scenario 1.

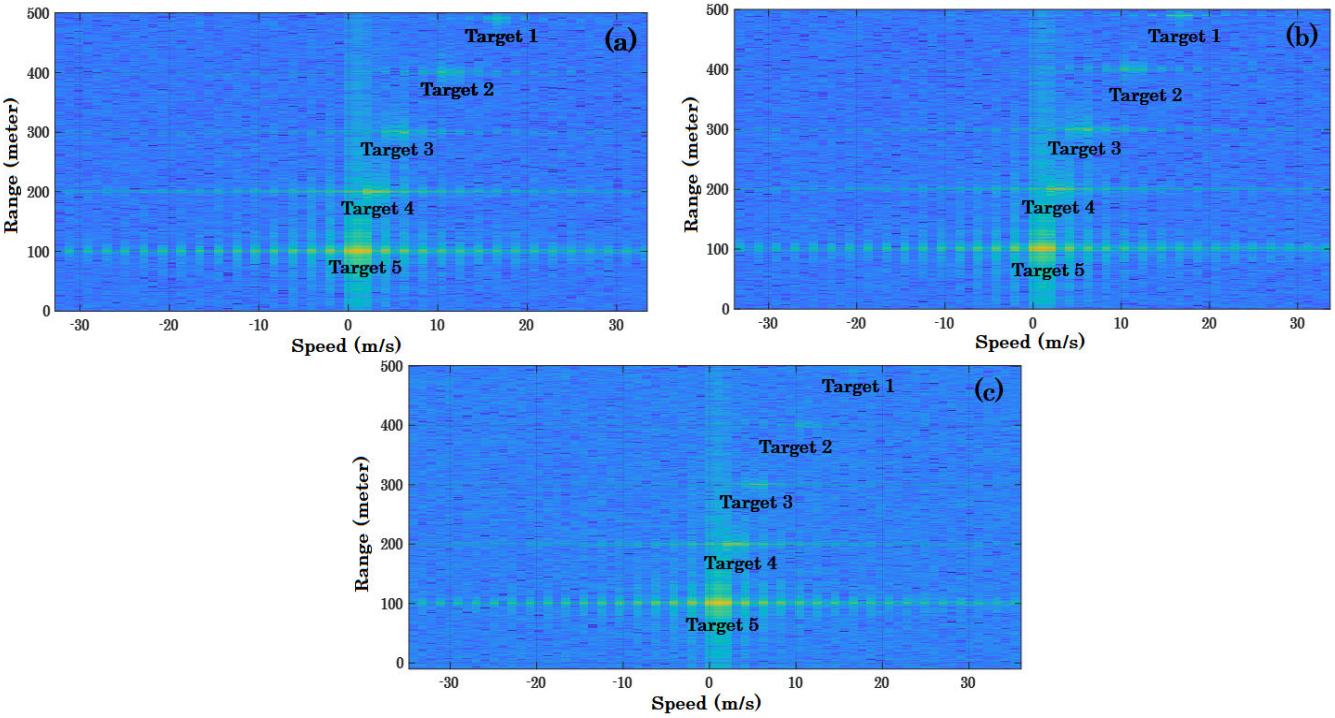

FIGURE 3. Range-Doppler measurements of LFMCW-RADAR under the influence of (a) mild rain only, (b) mild fog + cloud, and (c) mild rain, fog, cloud for Scenario 1.

signal is observed, for all the considered illuminated-targets, using LFMCW-PHRAD, as shown in Figure 4, in contrast with FMCW-RADAR, as shown in Figure 2(a).

This may be due to the optical treatment of the radar-signals before their transmission over the free space channel. It implies that a prolonged tracking-range is attainable with

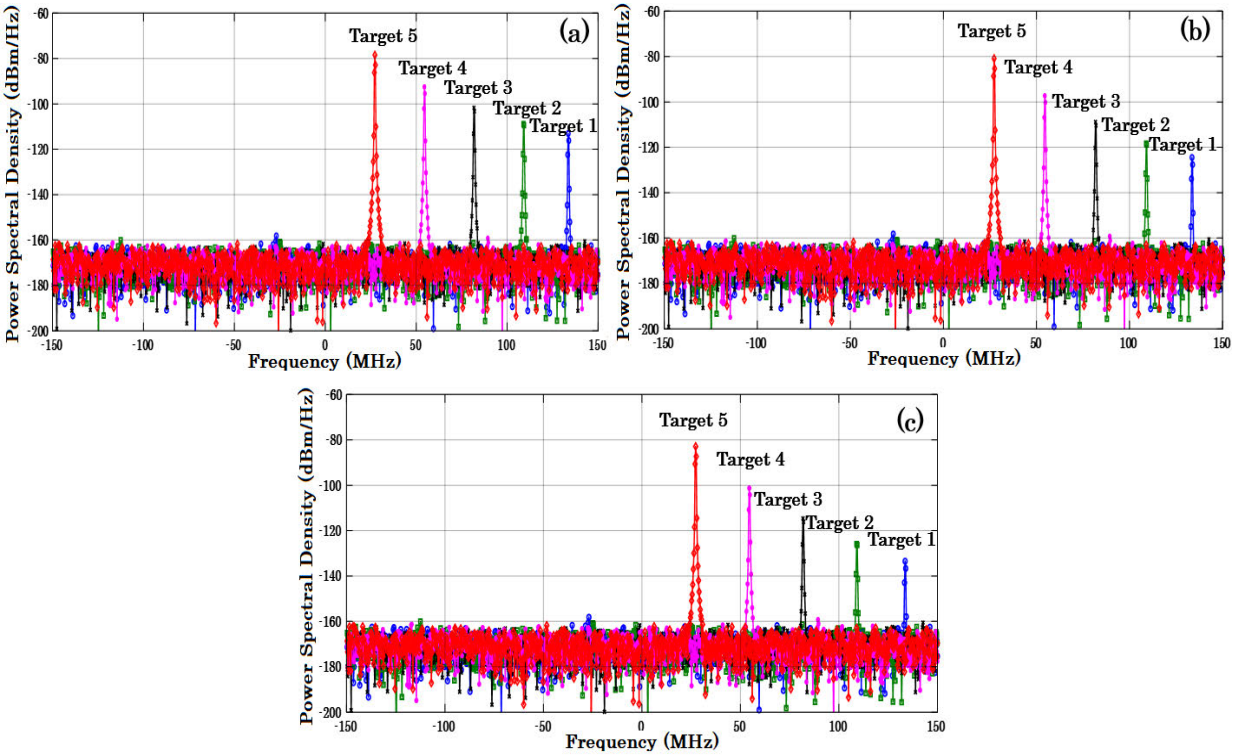

FIGURE 4. Power Spectral Density measurement of LFMCW-PHRAD at (a) Rain-fall rate = 10 mm/hr, (b) Rain-fall rate = 50 mm/hr, and (c) Rain-fall rate = 100 mm/hr for Scenario 2.

TABLE 2. Scenario-I.

Quantity	Target 1	Target 2	Target 3	Target 4	Target 5
Range	490 m	400 m	300 m	200 m	100 m
Velocity	40 Km/hr	60 Km/hr	80 Km/hr	90 Km/hr	96 Km/hr
Relative Velocity	16.66 m/s	11.11 m/s	5.55 m/s	2.77 m/s	1.11 m/s

the demonstrated PHRAD along with an accurate measurement of the target-velocities unambiguously up to a maximum target-range of 500 m.

Moreover, all the targets are easily detectable to a longer distance even under the impact of severe rain-fall rate compared to the conventional radar, as shown in Figure 5. It is also observed that the intensity of the beat signals reduces with the increase of the rain-fall rate shown in Figure 4. The impact of the severity level of the rain is observed marginal less up to a detection range of 100 m. But, beyond it, it increases with an intensity-loss of $\approx$ 5 dBm. This implies that the targets which are moving with high relative-velocity and at a longer distance from the point-of-observation, are more affected as the severity level of the rain increases. This shows that the detection-ability is highly dependent upon the distance, relative-velocity, operating frequency, and rain-fall rate as is apparent from the observations. However, the demonstrated laser-driven radar shows its ability to simultaneous measurement of the target-location and velocity to a longer distance ($\approx$ 500 m) accurately at a high rain-fall rate (100 mm/hr) in comparison with the LFMCW-RADAR.

The demonstrated laser-driven radar is further tested under the impact of fog and cloud collectively at different severity levels. The severity level of the occurrence of fog and cloud is measured by considering the amount of presence of water vapor-density in the atmosphere [19]. The results, as shown in Figure (6–7), observe that the intensity of the beat signals is significantly reduced under heavy fog as compared to mild fog and thus, limits the visibility-range. Moreover, the targets at longer distances are more affected, i.e. targets 1-4 experience an intensity-loss of 20 dBm to 7 dBm. Therefore, it becomes important to measure the unambiguous target-range and velocity accurately under the combined influence of fog, cloud, and rain, as shown in Figure 7. However, the demonstrated PHRAD offers a better detection range in contrast with the conventional microwave-radar.

VI. RCS-BASED MEASUREMENTS FOR NORMAL TRAFFIC-SCENARIOS

In the above-modeled scenarios, identical targets are considered. But, to assess a real traffic-scenario, different illuminated-targets with different radar cross-section is required to be tested. Subsequently, this section describes another scenario, i.e. Scenario 3, in which five mobile-targets (car, truck, motorbike, bicycle, and pedestrian) are modeled based on their measured RCS in conventional traffic scenes under the combined impact of fog, cloud, and rain at

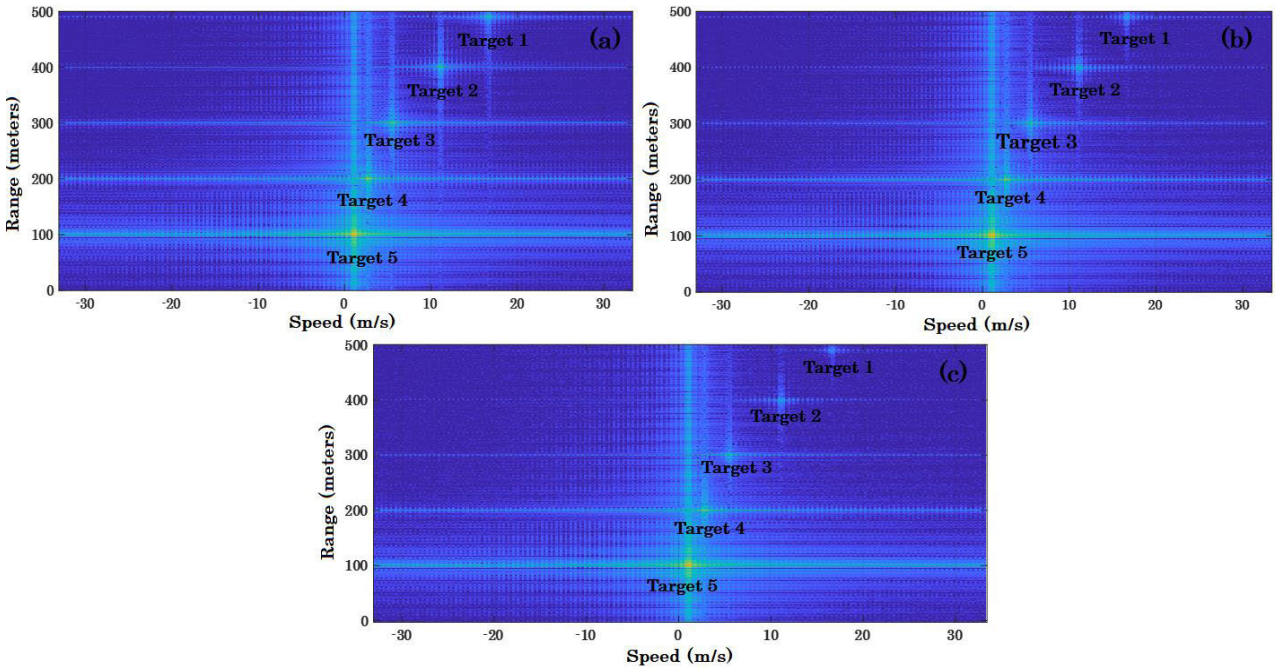

FIGURE 5. Range-Doppler measurements of LFMCW-PHRAD at (a) Rain-fall rate = 10 mm/hr, (b) Rain-fall rate = 50 mm/hr, and (c) Rain-fall rate = 100 mm/hr for Scenario 2.

TABLE 3. Scenario-2.

Quantity	Car	Truck	Motor Bike	Pedestrian	Bi-Cycle
Range	150 m	200 m	100 m	70 m	80 m
Velocity	96 Km/hr	80 Km/hr	60 Km/hr	5 Km/hr	25 Km/hr
Relative Velocity	1.11 m/s	5.55 m/s	11.11 m/s	26.38 m/s	20.83 m/s
RCS	20 dBsm	45 dBsm	7 dBsm	-10 dBsm	4 dBsm

rainfall rate of 50 mm/hr with liquid water-density of 2.5. Moreover, the multiple-targets defined in this scenario are associated with different RCS depending upon their dimensions and their current location from the radar-equipped vehicle. The RCS for the car and truck are calculated as a function of distance from the radar-equipped vehicle using equations (5) and (6). While for the small targets, like the motorbike, bicycle, and pedestrian, the RCS are taken 7 dB, 4 dBm, and −10 dBm, respectively. Besides it, in this scenario, each target is modeled to travel at a different speed and different distance from the radar-equipped vehicle, as shown in Table 3. Moreover, the performance of both the radar systems is evaluated to a maximum range of 200 m only in this scenario as the maximum range-detection for microwave radar is drastically reduced under severe weather conditions as described in Section V. Also, the small targets having low RCS are challenging to detect using conventional radar under the combined impact of the weather conditions at strong regimes.

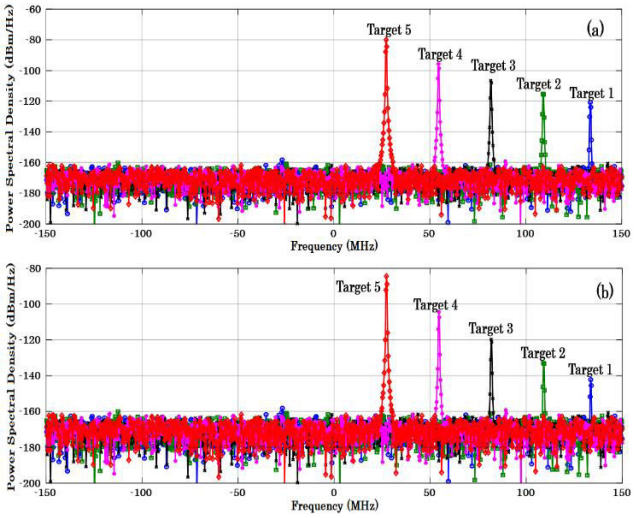

FIGURE 6. Power Spectral Density measurements of LFMCW-PHRAD under the influence of fog + cloud with (a) Liquid water-density = 1, and (b) Liquid water-density = 2.5.

Better visibility-range for all the defined-targets with FMCW-PHRAD is observed under the combined influence of the considered harsh weather factors compared to the conventional radar, as shown in Figure 8. Further, it is observed that small-size targets like pedestrians, motorbikes, and bicycles are better localized with the laser-driven radar compared to the conventional radar. Moreover, it shows that the detection-ability of the radar depends upon one more factor, i.e. the radar cross-section along with the distance,

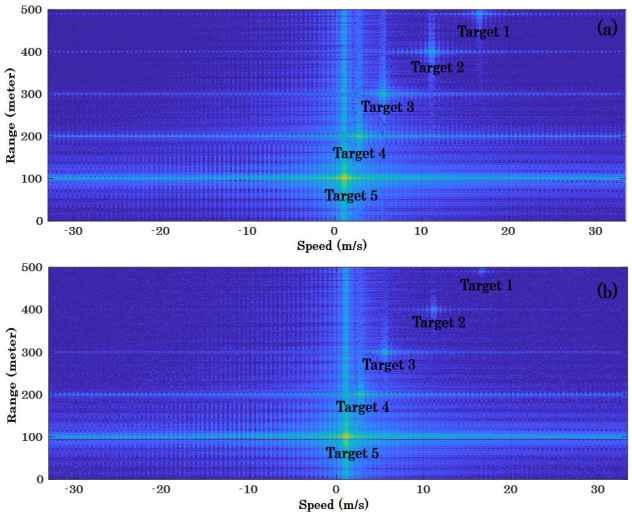

FIGURE 7. Range-Doppler measurements of LFMCW-PHRAD under the influence of fog + cloud with (a) Liquid water-density = 1, and (b) Liquid water-density = 2.5.

relative-velocity, operating frequency, and weather factors. This implies that the higher the RCS of an illuminated target, high is the intensity of the returned pulses. Moreover, the signal-to-noise ratio (SNR) measurements for both the demonstrated radar systems under clear and severe weather conditions (under the influence of the combined impact of the considered environment factors in this work) are presented in Table 4.

TABLE 4. Signal-to-Noise (SNR) Ratio Measurements.

PHRAD			
S.NO	Distance (m)	SNR (Clear Weather)	SNR (Severe Weather)
1	100	55.48 dB	48.25 dB
2	200	49.02 dB	40.37 dB
3	300	39.67 dB	33.00 dB
4	400	21.75 dB	17.00 dB
5	500	19.53 dB	14.14 dB
Microwave Radar			
S.NO	Distance (m)	SNR (Clear Weather)	SNR (Severe Weather)
1	100	51.55 dB	42.5 dB
2	200	47.11 dB	36.17 dB
3	300	23.29 dB	13.4 dB
4	400	15.66 dB	3.17 dB
5	500	5.56 dB	0 dB

VII. RCS-BASED MEASUREMENTS FOR COMPLEX TRAFFIC-SCENARIOS

Due to the dependency of RCS of illuminated targets over the intensity of the echoes, the work is extended to assess the RCS-based target-detection for complicated traffic-scenarios in the presence of atmospheric fluctuations. To accomplish this objective, two complex real-time road-scenes are

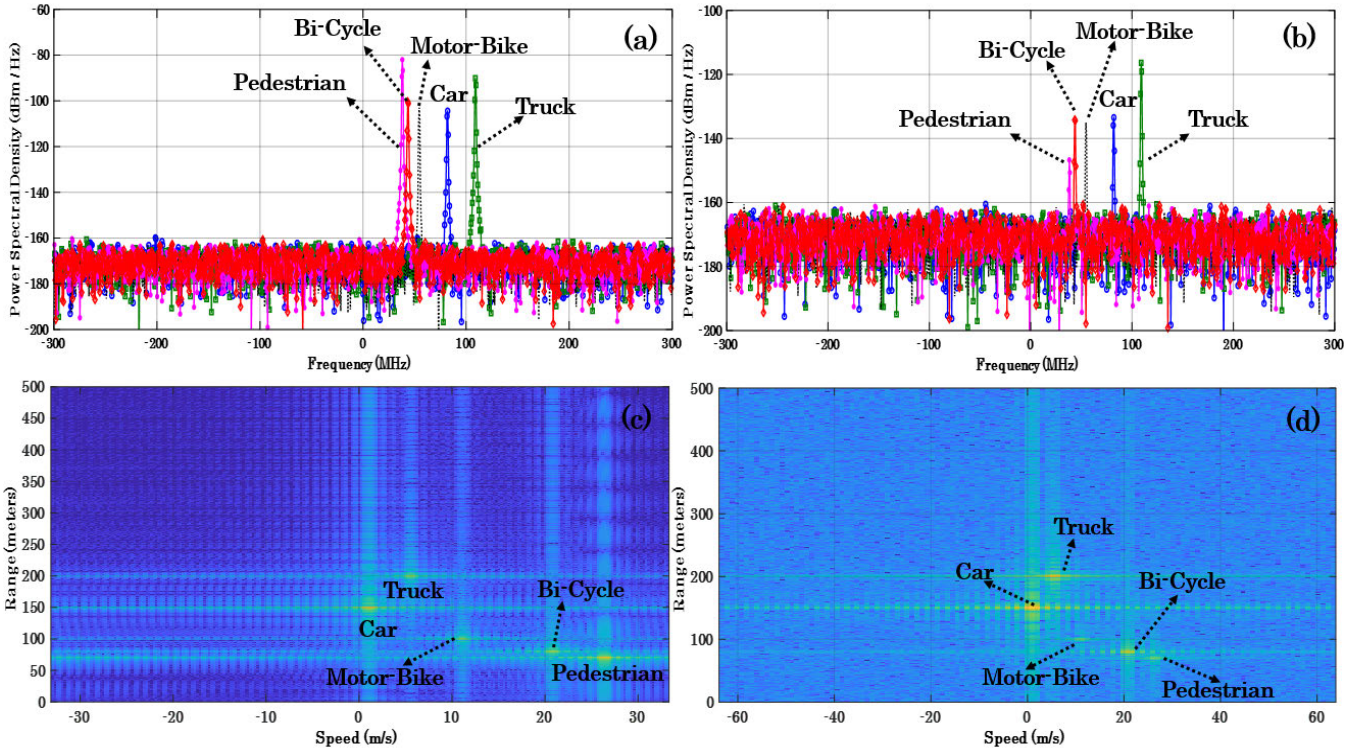

FIGURE 8. RCS-based measurements of Power Spectral Density and Range-Speed mapping for (a, c) LFMCW-PHRAD, and (b, d) LFMCW-RADAR at Rainfall rate = 50 mm/hr and liquid water-density = 2.5.

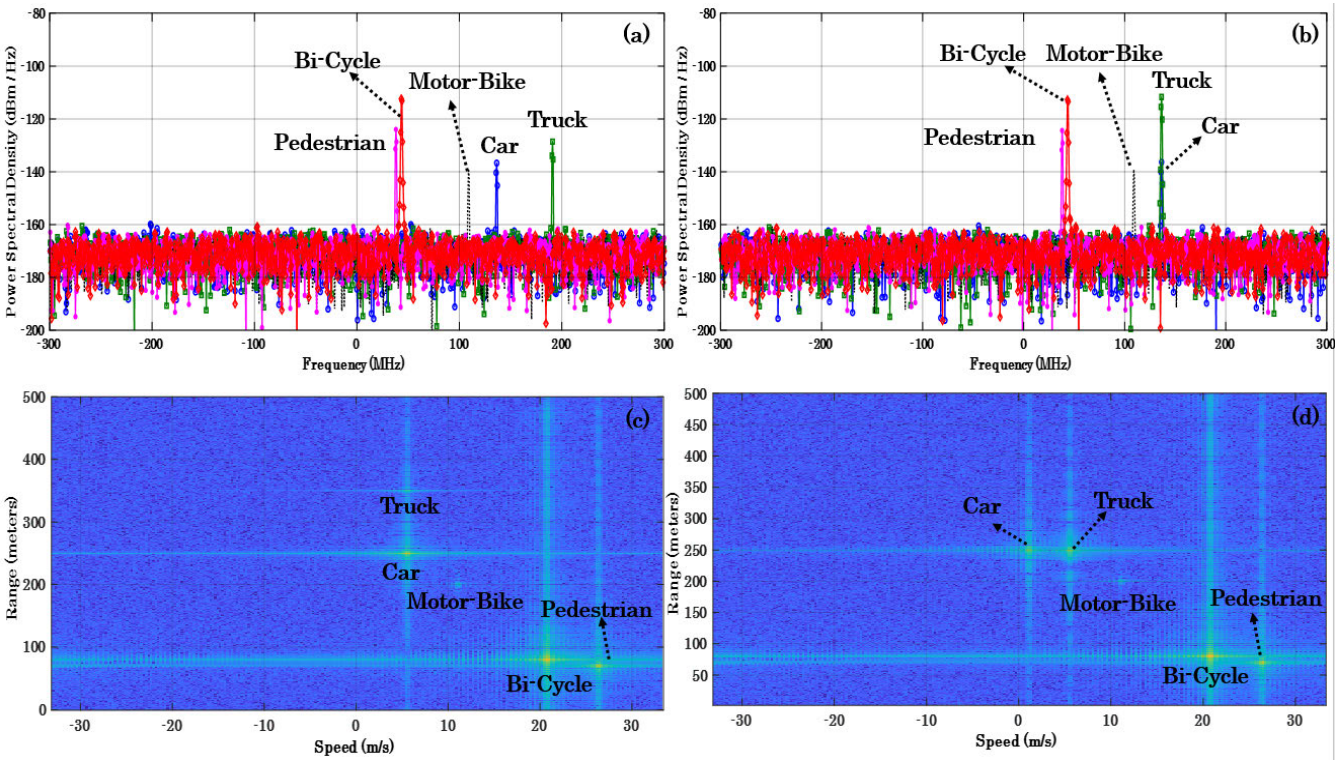

FIGURE 9. RCS-based measurements of Power Spectral Density and Range-Speed mapping of LFMCW-PHRAD for (a, c) Scenario 4, and (b, d) Scenario 5 at Rainfall rate = 50 mm/hr and liquid water-density = 2.5.

modeled in Scenarios 4–5. Both the scenarios are tested for the demonstrated PHRAD only as it performs better in contrast to the conventional radar as discussed in previous sections. Scenario 4 illustrates the traffic scene in which the targets are moving at different distances with the same velocity [30]. In this scenario, the large-size targets, like car and truck are considered at 250 m and 350 m respectively from the radar-equipped vehicle but are traveling with the same velocity of 80 km/hr. However, the small-size targets are modeled to travel at different velocities (Motorbike = 60 km/hr, Bicycle = 25 km/hr, and Pedestrian = 5 km/hr) at a different distance (Motorbike = 200 m, Bicycle = 80 m, and Pedestrian = 70 m). This assumption is demonstrated as the difference of relative-velocity between the small- and large-targets is very high, especially in the case of bicycle and pedestrian. For Scenario 4, the outcomes show the simultaneous measurements of the target-range along with the radial-velocities unambiguously in the modeled complex traffic-scenarios for the demonstrated FMCW-PHRAD under the severe atmospheric fluctuations as illustrated in Figure 9 (a, c). Moreover, the impact of the atmospheric fluctuations can be easily observed from their respective measured intensity of beat signals as shown in Figure 9 (a).

In Scenario 5, the large-size targets are moving at the same distance of 250 m from the radar-equipped vehicle at different velocities (Car = 96 km/hr, and Truck = 80 km/hr). The small targets are still moving at the same velocities and the same distance as defined in Scenario 4. It is observed that the beat frequency of the car and truck is overlapping which is due to the Doppler Effect as both the targets are traveling at the same distance as shown in Figure 9 (b). However, a significant difference in the intensity of their respective beat signals is observed due to different radar cross-section associated with them. This overlapping may be ratified by measuring the incident angle of the reflected echoes from both the targets. Conversely, the range-Doppler mapping shows a clear detection of all the considered targets as shown in Figure 9 (d) in the presence of heavy fog, cloud, and rain.

VIII. CONCLUSION

This work demonstrates an LFMCW-PHRAD radar to perform simultaneous and unambiguous measurements of range and velocity for different complex real-time traffic-scenarios employed with multiple-mobile targets having divergent radar cross-section under atmospheric fluctuations. The demonstrated photonic-radar under the atmospheric variations is also compared to the conventional microwave-radar to validate its tracking-ability. The observations reveal that the laser-driven radar offers improved detection-range and velocity, accurate target-location, and target-identification with high range-resolution. Moreover, the outcomes show a significant influence of the individual and combined impact of the considered weather factors on the tracking-range of the radar. It is due to the presence of the liquid water-density due to fog, clouds, and the rainfall rate. Furthermore, an RCS-based target-tracking is also carried out and investigated comprehensively to differentiate and locate the multiple targets in complex traffic-scenarios.

In the earlier reported work, the observations are recorded in some random traffic-scenarios using a fixed-location-based radar without considering the impact of atmospheric variations in detail. On the other hand, in this work, the LFMCW-PHRAD is installed on a mobile vehicle to observe different mobile targets differentiated in terms of their associated RCS to demonstrate different non-complex and complex traffic-scenarios. However, the exhibit work has not tested the influence of the clutter response, which may arise due to the multipath propagation of the returning echoes.

Moreover, the authors believe that there may be some variations in real-time experiments in contrast to the numerical simulation measurements. However, the demonstrated work may help the researchers in developing laser-driven radar systems experimentally to attain high range- and imagery-resolution along with prolonged detection-range to realize the state-of-the-art self-driving vehicles and other surveillance-related applications. Therefore, we believe that the extension of this work demonstrated in a simulation environment can be accomplished in the future to perform experimental and field-trials-based measurements.

REFERENCES

[1] K. Bimbraw, "Autonomous cars: Past, present and future—A review of the developments in the last century, the present scenario and the expected future of autonomous vehicle technology," in *Proc. 12th Int. Conf. Informat. Control, Autom. Robot.*, Colmar, France, vol. 1, 2015, pp. 191–198.

[2] *Self-Driving Cars Explained*. Accessed: Nov. 2020. [Online]. Available: https://www.ucsusa.org/clean-vehicles/how-self-driving-cars-work

[3] S. Thrun, "Toward robotic cars," *Commun. ACM*, vol. 53, no. 4, pp. 99–106, Apr. 2010.

[4] A. Mukhtar, L. Xia, and T. B. Tang, "Vehicle detection techniques for collision avoidance systems: A review," *IEEE Trans. Intell. Transp. Syst.*, vol. 16, no. 5, pp. 2318–2338, Oct. 2015.

[5] *World Report on Road Traffic Injury Prevention: Main Messages*, World Health Org., Geneva, Switzerland, 2020.

[6] C. T. Allen, S. K. Chong, Y. Cobanoglu, and S. Gogineni, "Development of a 1319-nm laser radar using fiber optics and RF pulse compression," Univ. Kansas, Lawrence, KS, USA, Tech. Rep. ITTC-RSL-FY2002-TR-18680-01, 2002.

[7] W.-J. Yang, J.-G. Zhao, X.-P. Du, Z.-Y. Zeng, and Q. Wang, "Laser diode transmitter for laser radar based on FM ranging principles," in *Proc. Int. Symp. Photoelectronic Detection Imag., Optoelectronic Syst. Design, Manuf., Test.*, Sep. 2007, Art. no. 662408-9.

[8] H. Zhang, J. Li, T. Wang, H. Lin, Z. Zheng, Y. Li, and Y. Lu, "A manifold learning approach to urban land cover classification with optical and radar data," *Landscape Urban Planning*, vol. 172, pp. 11–24, Apr. 2018.

[9] X. Tong, X. Luo, S. Liu, H. Xie, W. Chao, S. Liu, S. Liu, A. N. Makhinov, A. F. Makhinova, and Y. Jiang, "An approach for flood monitoring by the combined use of Landsat 8 optical imagery and COSMO-SkyMed radar imagery," *Elsevier, J. Photogramm. Remote Sens.*, vol. 136, pp. 144–153, Feb. 2018.

[10] W. Shena, M. Lia, C. Huang, X. Taod, and A. Wei, "Annual forest aboveground biomass changes mapped using ICESat/GLAS measurements in China," *Agricult. Forest Meteorol.*, vol. 259, pp. 23–38, Sep. 2018.

[11] L. Poggio and A. Gimona, "Assimilation of optical and radar remote sensing data in 3D mapping of soil properties over large areas," *Sci. Total Environ.*, vol. 579, pp. 110–1094, Feb. 2017.

[12] I. Skog and P. Handel, "In-car positioning and navigation technologies—A survey," *IEEE Trans. Intell. Transp. Syst.*, vol. 10, no. 1, pp. 4–21, Mar. 2009.

[13] R. Mautz, "Combination of indoor and outdoor positioning," in *Proc. 1st Int. Conf. Mach. Control Guid.*, 2008, pp. 79–87.

[14] S. Haykin, "Cognitive radar: A way of the future," *IEEE Signal Process. Mag.*, vol. 23, no. 1, pp. 30–40, Jan. 2006.

[15] J. B. Tsui, *Digital Techniques for Wideband Receivers*, 2nd ed. Rijeka, Croatia: SciTech, 2004.

[16] J. A. Scheer and J. L. Kurtz, *Coherent Radar Performance Estimation*. Norwood, MA, USA: Artech House, 1993.

[17] *Specific Attenuation Model for Rain for Use in Prediction Methods*, document ITU-R P.838-3, 2005.

[18] *Attenuation Due to Clouds and Fog*, document ITU-R P.840-6, 2013.

[19] *Attenuation by Atmospheric Gases*, document ITU-R P.676-11, 2016.

[20] T. Peynot, J. Underwood, and S. Scheding, "Towards reliable perception for unmanned ground vehicles in challenging conditions," in *Proc. IEEE/RSJ Int. Conf. Intell. Robots Syst.*, Oct. 2009, pp. 1170–1176.

[21] R. H. Rasshofer, M. Spies, and H. Spies, "Influences of weather phenomena on automotive laser radar systems," *Adv. Radio Sci.*, vol. 9, pp. 49–60, Jul. 2011.

[22] J. Wojtanowski, M. Zygmunt, M. Kaszczuk, Z. Mierczyk, and M. Muzal, "Comparison of 905 nm and 1550 nm semiconductor laser rangefinders' performance deterioration due to adverse environmental conditions," *Opto-Electron. Rev.*, vol. 22, no. 3, pp. 183–190, Jan. 2014.

[23] S. Hasirlioglu, A. Riener, W. Huber, and P. Wintersberger, "Effects of exhaust gases on laser scanner data quality at low ambient temperatures," in *Proc. 4th IEEE Intell. Vehicles Symp.*, Los Angeles, CA, USA, Jun. 2017, pp. 1708–1713.

[24] M. Bijelic, T. Gruber, and W. Ritter, "A benchmark for lidar sensors in fog: Is detection breaking down?" in *Proc. 4th IEEE Intell. Vehicles Symp.*, Changshu, China, Jun. 2018, pp. 760–767.

[25] M. Bijelic, T. Gruber, and W. Ritter, "A benchmark for lidar sensors in fog: Is detection breaking down?" in *Proc. 4th IEEE Intell. Vehicles Symp.*, Changshu, China, Jun. 2018, pp. 26–30.

[26] A. Filgueira, H. González-Jorge, S. Lagüela, L. Díaz-Vilariño, and P. Arias, "Quantifying the influence of rain in LiDAR performance," *Measurement*, vol. 95, pp. 143–148, Jan. 2017.

[27] I. Gultepe, R. Tardif, S. C. Michaelides, J. Cermak, A. Bott, J. Bendix, M. D. Müller, M. Pagowski, B. Hansen, G. Ellrod, W. Jacobs, G. Toth, and S. G. Cober, "Fog research: A review of past achievements and future perspectives," *Pure Appl. Geophys.*, vol. 164, nos. 6–7, pp. 1121–1159, Jun. 2007.

[28] V. Sharma and S. Sergeyev, "Range detection assessment of photonic radar under adverse weather perceptions," *Opt. Commun.*, vol. 472, Oct. 2020, Art. no. 125891, doi: 10.1016/j.optcom.2020.125891.

[29] V. Sharma, S. Sergeyev, L. Kumar, and H. J. Kbashi, "Range-speed mapping and target-classification measurements of automotive targets using photonic-radar," *Opt. Quantum Electron.*, vol. 52, no. 10, Oct. 2020, doi: 10.1007/s11082-020-02557-5.

[30] H.-S. Lim, J.-E. Lee, H.-M. Park, and S. Lee, "Stationary target identification in a traffic monitoring radar system," *Appl. Sci.*, vol. 10, no. 17, p. 5838, Aug. 2020.

[31] D. Felguera-Martín, J. T. González-Partida, P. Almorox-González, and M. Burgos-García, "Vehicular traffic surveillance and road lane detection using radar interferometry," *IEEE Trans. Veh. Technol.*, vol. 61, no. 3, pp. 959–970, Jan. 2012.

[32] M. I. Hussain, S. Azam, F. Munir, Z. Khan, and M. Jeon, "Multiple objects tracking using radar for autonomous driving," in *Proc. IEEE Int. IoT, Electron. Mechatronics Conf. (IEMTRONICS)*, Vancouver, BC, Canada, Sep. 2020, pp. 1–4, doi: 10.1109/IEMTRONICS51293.2020.9216363.

[33] K. Ramasubramanian and K. Ramaiah, "Moving from legacy 24 GHz to state-of-the-art 77-GHz radar," *ATZelektronik worldwide*, vol. 13, no. 3, pp. 46–49, May 2018.

[34] C. L. Andrews, L. R. Phillips, and Y. C. Hopen, *Laser Beam Scintillation With Applications*. Bellingham, WA, USA: SPIE, 2001.

[35] A. A. Farid and S. Hranilovic, "Outage capacity optimization for free-space optical links with pointing errors," *J. Lightw. Technol.*, vol. 25, no. 7, pp. 1702–1710, Jul. 2007.

[36] S. Gao, M. O'Sullivan, and R. Hui, "Complex-optical-field photonic-radar system for range and vector velocity measurement," *Opt. Exp.*, vol. 20, no. 23, pp. 25867–25875, Nov. 2012.

[37] P. Adany, C. Allen, and R. Hui, "Chirped photonic-radar using simplified homodyne detection," *J. Lightw. Technol.*, vol. 27, no. 16, pp. 3351–3357, Aug. 2009.

[38] N. Yamada, Y. Tanaka, and K. Nishikawa, "Radar cross section for pedestrian in 76GHz band," in *Proc. Eur. Microw. Conf.*, vol. 2, 2005, pp. 46–51.

[39] R. Schneider, H.-L. Blocher, and K. M. Strohm, "KOKON–automotive high frequency technology at 77/79 GHz," in *Proc. Eur. Radar Conf.*, Munich, Germany, Oct. 2007, pp. 247–250.

[40] H. Suzuki, "Radar cross section of automobiles for millimeter wave band," *JARI Res. J.*, vol. 22, no. 10, pp. 475–478, 2000.
[41] N. Yamada, "Three-dimensional high resolution measurement of radar cross section for car in 76 GHz band," *R D Rev. Toyota Central R D Labs.*, vol. 36, no. 2, pp. 1–2, 2001.
[42] K. Schuler, D. Becker, and W. Wiesbeck, "Extraction of virtual scattering centers of vehicles by ray-tracing simulations," *IEEE Trans. Antennas Propag.*, vol. 56, no. 11, pp. 3543–3551, Nov. 2008.
[43] C. Karnfelt, A. Peden, A. Bazzi, G. El Haj Shhade, M. Abbas, and T. Chonavel, "77 GHz ACC radar simulation platform," in *Proc. 9th Int. Conf. Intell. Transp. Syst. Telecommun., (ITST)*, Oct. 2009, pp. 209–214, doi: 10.1109/itst.2009.5399354.
[44] R. L. Olsen, D. V. Rogers, and D. B. Hodge, "The aR^b relation in the calculation of rain attenuation," *IEEE Trans. Antennas Propag.*, vol. 26, no. 2, pp. 318–329, Mar. 1978.

VISHAL SHARMA (Senior Member, IEEE) received the Masters of Technology degree in electronics and communication from IKG Punjab Technical University, India, in 2007, and the Ph.D. degree in engineering, in 2013.

Since 2009, he has been deputed as an Associate Professor with the State Government Engineering Campus after the name of Bhagat Singh State Technical Campus (SBSSTC), Punjab, India. He is currently a Marie Skłodowska Curie Fellow with the School of Engineering and Applied Science, Aston Institute of Photonics Technologies (AiPT), Aston University, Birmingham, U.K. His contributions including 71 research papers have been featured in several reputed international journals and conferences, such as *Optics & Lasers in Engineering* (Elsevier), *AEU* (Elsevier), IEEE Access, *Wireless Networks* (Springer), *Soft Computing* (Springer), Wiley, IEEE, IET, and Taylor & Francis. His research interests include ultra-short pulse laser designing, photonic radar, radio over fiber (RoF) systems, photonic-microwave networks, free space optics (FSO), inter-satellite optical wireless systems (IsOWC), and wireless sensor networks (WSN).

LOVE KUMAR received the Ph.D. degree in engineering from IKG Punjab Technical University, Punjab, India, in 2019. He is currently working as an Assistant Professor with the Department of Engineering and Communication, DAV Institute of Engineering and Technology (DAVIET), affiliated with IKG Punjab Technical University. He has published more than 30 research papers in several reputed international journals and conferences, such as IEEE, Elsevier, Springer, and Taylor & Francis. His research interests include hybrid optical and wireless communication systems/networks, photonics-based wireless systems/networks, and mobile communication systems/networks.